Proceedings of ASME Turbo Expo 2011
GT2011
June 6-10, 2011, Vancouver, British Columbia, Canada

GT2011-45951

VALIDATION OF A COUPLED FLUID/SOLID HEAT TRANSFER METHOD

Jose M. Chaquet, Roque Corral*, Guillermo Pastor
Technology and Methods Department
Industria de TurboPropulsores S.A.
28830 Madrid, Spain
e-mails: Jose.Chaquet@itp.es,
Guillermo.Pastor@itp.es, Roque.Corral@itp.es

Jesus Pueblas
School of Aeronautics
UPM
28040 Madrid, Spain
e-mail: Jesus.Pueblas@upm.es

D. D. Coren
Thermo-Fluid Mechanics Research Center
Dept. of Engineering and Design
University of Sussex, Brighton, BN1 9QT
e-mail: d.d.coren@sussex.ac.uk

ABSTRACT

A coupled method for solid/fluid steady heat transfer calculations is presented. The results of the fully coupled and uncoupled simulations are compared with the experimental data obtained for the front and rear stator well of a turbine. Several cooling mass flow rates have been considered. The uncoupled methodology is described as well and the accuracy of the results for both approaches is discussed. It is concluded that even if the uncoupled approach it is conducted carefully, the coupled method is more accurate since it removes some hypotheses inherent to the uncoupled approach.

NOMENCLATURE

Symbols

$d\mathbf{A}$	Differential area at boundaries
$\mathbf{F}$	Sum of inviscid and viscous fluxes
$\mathbf{n}$	Local normal vector to the boundary surface
$\mathbf{q}$	Heat flux vector $\left[Wm^{-2}\right]$
$\mathbf{U}$	Vector of conservative variables
a	Disc inner radius $[m]$
b	Disc outer radius $[m]$
g_{eq}	Volumetric force field (equivalent gravity force)
h	Heat transfer coefficient $\left[Wm^{-1}K^{-1}\right]$
k	Thermal conductivity $\left[Wm^{-1}K^{-1}\right]$
$\dot{m}$	Mass flow $\left[kg \cdot s^{-1}\right]$
Q	Volumetric heat sources $\left[Wm^{-3}\right]$
q	Normal component of the heat flux vector $\left[Wm^{-2}\right]$
T_{ref}	Reference temperature for convective boundary condition
T_{hot}	Hottest temperature in the computational domain $[K]$
T_{cold}	Colder temperature in the computational domain $[K]$
T_{aw}	Adiabatic wall temperature $[K]$
T_w	Metal wall temperature $[K]$
T_∞	Static temperature of the surrounding fluid $[K]$
T_T	Stagnation temperature $[K]$
U_∞	Characteristic velocity
Ω	Flow domain
Σ	Flow domain boundary
μ	Fluid viscosity $\left[kg \cdot m^{-1}s^{-1}\right]$
ρ	Density $\left[kg \cdot m^{-3}\right]$
ω	Rotation speed $\left[rad \cdot s^{-1}\right]$

Dimensionless

Ec	Eckert Number
C_w	Nondimensional mass flow, $\dot{m}b^{-1}\mu^{-1}$
Gr	Grashof Number
M	Mach Number
Re	Reynolds Number
Re_ϕ	Rotational Reynolds Number, $\rho\omega b^2\mu^{-1}$
θ	Nondimensional temperature

Subscripts

0	Free disc value at equal Re_ϕ

*Also associate professor at the Department of Engine Propulsion and Fluid Dynamics of the School of Aeronautics, UPM

$EucError$	Error using Euclidean norm
$MaxError$	Error using Max norm
ent	Entrained flow value
exp	Experimental data
f	Fluid domain
m	Metal/solid domain

INTRODUCTION

Turbomachinery design requirements are every day more and more demanding in terms of performance, efficiency and component life. To address these requirements, more powerful simulation tools are needed to accurately predict complex physics phenomena quick enough to be used during the standard design process. The prediction of metal temperatures in cooled and uncooled turbines falls under this category.

Thermal models usually use simple tuned correlations to account for convection phenomena. Although the computational power required is low, because convecting correlations are implemented as boundary conditions in the thermal solver, this methodology poses some set-up difficulties and a not negligible lack of accuracy. The mean advantage of this approach is that tailored analysis tools for this type of analysis may yield a very short turnaround time. With rapid progress of Computational Fluid Dynamics (CFD) and computer power, CFD has proven to be useful for improving metal temperature predictions. Three types of approaches can be found in the literature in using CFD solutions to solid/fluid heat transfer computations: conjugate heat transfer analysis, coupled thermal/CFD procedure and uncoupled thermal/CFD analysis.

In conjugate heat transfer analysis, only one solver is used dealing both with fluid and metal domains. Several applications can be found in the literature such as a real turbine rotor-stator system simulation [14] or internally cooled turbine blade applications [11]. This methodology is suitable neither for steady-state nor transient flight cycles because the computational cost could be prohibitive. The use of synchronized thermal and fluid solvers, irrespectively of whether the solvers are actually the same or not, imposes severe restrictions since the characteristic times of the solid and the fluid differ by several orders of magnitude and therefore explicit time-accurate CFD solvers need to be run for very long times because of its coupling with relatively inexpensive thermal solvers. The distinction in the literature between conjugate and coupled methods is somehow arbitrary since it refers to the global iteration method. Coupled methods usually refer to loosely coupled methods where two different codes are coupled through their boundaries at prescribed time intervals which are selected by accuracy, not stability restrictions, and therefore are much more efficient than conjugate gradient methods. The time scale dictated by the physical time intervals, which is controlled by the diffusion time of the solid, is very large compared with the residence time of fluid. This means the problem is quasi-stationary from the point of view of the fluid and steady CFD analysis are valid even for thermal transient problems. Moreover, existing CFD and thermal codes may be reused with minor modifications, easing the maintenance and development of these codes.

The main difference between coupled and uncoupled methods is the number of CFD simulations needed. In the coupled approach, for several time instants fixed usually by the solid transient, a CFD simulation is performed until a converged is reached, i.e. the continuity of temperature and heat flux is achieved at wall interfaces. Some examples of coupled approaches can be seen in [16, 13, 10]. More recently, some efficient simulations for engineering applications have been done [15] where only the energy equation is solved in the fluid part while the flow is frozen during the thermal coupling process for specified time intervals.

In the uncoupled approach, a limited number of CFD simulations are performed at key engine operation conditions to produce boundary conditions for traditional thermal analysis. Some examples for turbine cavities can be seen in [12, 1]. Although great computational cost is saved in this approach, some simulations are not accurate enough. Uncoupled analysis make use of some *a priori* knowledge about the physics of the problem that sometimes is not fulfilled.

In the present work a coupled method for solid/fluid heat transfer calculations is presented for steady simulations. The method is validated using a 3D stator with its corresponding front and rear cavities for which experimental data are available. Several cooling mass flow rates have been considered. The uncoupled methodology is described as well and the discrepancies of the results for both approaches are discussed. Results have been compared against experimental data taken from the EU FP6 STREP project code-named as MAGPI (Main Annulus Gas Path Interactions) [7], whose main objective is to improve the current understanding of the secondary and main streams flows interactions.

NUMERICAL MODEL

Resolution of the governing equations

Before describing the coupled and uncoupled approaches, a brief description of the CFD and thermal solvers is given.

The CFD code known as Mu^2s^2T [4] solves the compressible Navier-Stokes equations in conservative form for an arbitrary control volume, which may be written in compact form as

$$\frac{d}{dt}\int_{\Omega}\mathbf{U}d\Omega+\int_{\Sigma}\mathbf{F}(\mathbf{U}).d\mathbf{A}=0 \qquad (1)$$

where $\mathbf{U}$ is the vector of conservative variables, $\mathbf{F}$ the sum of the inviscid and viscous fluxes, Ω the flow domain, Σ its boundary

and $d\mathbf{A}$ the differential area pointing outward to the boundary. The solver uses hybrid unstructured grids [3] to discretise the spatial domain and may contain cells with an arbitrary number of faces. The solution vector is stored at the vertexes of the cells. Turbulence effects are modelled using either the $k-\omega$ two-equation turbulence model advocated by Wilcox [18] or the algebraic Baldwin-Lomax [2] model. The basic time-stepping scheme is an explicit five-stage Runge-Kutta scheme, where the artificial viscosity and the viscous terms are evaluated only in three stages. Local time stepping is used to enhance the convergence acceleration. The residuals are smoothed implicitly by a Jacobi iteration scheme in order to increase the support of the space discretisation as well. Low Mach number preconditioning is also used to accelerate convergence to steady state. Multigrid and parallel techniques are used to reduce the turnaround time.

The thermal code, known as *Mephisto,* is as well an in house solver [8] that solves the Heat Diffusion equation for a solid, that in integral form may be written as

$$\int_\Omega \rho c \frac{dT}{dt}\, d\Omega = \int_\Sigma \mathbf{q}\cdot d\mathbf{A} + \int_\Omega Q\, d\Omega\,, \tag{2}$$

where $\mathbf{q} = k\nabla T$ is the heat flux, Q is the volumetric heat sources, Ω the solid domain, Σ its boundary and $d\mathbf{A}$ the differential area pointing outward to the boundary.

Dirichlet and Newmann boundary conditions may be used to specify either the temperatures or the heat flux at the walls. The spatial discretization strategy is exactly the same than that of the CFD solver. The resulting set of equations is solved using a SOR method. Transients are marched in time using an implicit Crank-Nicholson scheme. The system features a fairly large number of boundary conditions and capabilities which are not described here because there are not relevant for the present work. The interested reader may find the details in [8]

Simplified fluid/solid boundary conditions

Thermal codes usually use a simple relationship to link the solid with the fluid that may be expressed as

$$q = h\,(T_{aw} - T_w) \tag{3}$$

where, h is the heat transfer coefficient, q is the normal component of the heat flux vector to the surface, T_w is the metal temperature at the wall and T_{aw} is usually referred to as the adiabatic wall temperature, that for homogeneous flows is very close to the stagnation temperature of the stream, $T_{aw} \simeq T_T$, and for low Mach number flows ($M_\infty \ll 1$) $T_{aw} \simeq T_\infty$, where T_∞ is the static temperature of the surrounding fluid.

Equation (3) is known as the Newton's law and was initially derived empirically. It states a linear relationship between the heat flux at the wall and the temperature difference between the fluid and the wall. Navier-Stokes equations are a non linear set on PDEs and therefore Eq. (3) may only be valid under certain hypothesis or for some canonical flows. Essentially, Newton's law only holds if the energy equation decouples from the momentum equation. This is in general only true for low-speed flows ($M_\infty = \sqrt{\gamma R_g T_\infty} \ll 1$) subject to small temperature differences ($(T_w - T_\infty)/T_\infty \ll 1$) and in the absence of buoyancy effects ($Gr^{1/2}/Re \propto (\Delta T/T_\infty)((g_{eq}L_c)^{1/2}/U_\infty) \ll 1$). Moreover it is necessary to require linearity for the energy equation. This condition is fulfilled for small Eckert numbers, i.e. $Ec = U_\infty^2/c_p(T_w - T_\infty) \ll 1$. It is usually assumed that the heat transfer coefficient is a function of the position, $h = h(\mathbf{x})$. However non uniform flows for which $T_{aw} = T_{aw}(\mathbf{x})$ are much less common, although non-uniformities in principle do not destroy the linearity of the problem.

Cavity flows do not fulfill most, if any, of the aforementioned conditions. It is even difficult to envision which is the exact meaning of some parameters, like the characteristic velocity, U_∞, within a cavity. Moreover the flow is inherently non-uniform since it is necessary to deal at least with the total temperatures of the main stream and the sealing flow, which are significantly different.

In order to obtain a better accuracy, a logical improvement of Eq. (3) is to use local values of h and T_{aw}, i.e. different values for each point at the boundary surfaces. In complex flows, like in a turbine cavity, it is difficult to define a unique adiabatic wall temperature for the entire fluid cavity. Using a correct value for T_{aw} is as important as the heat transfer coefficient h for computing correct heat fluxes at the wall. Then, if the heat transfer coefficient is considered constant at each wall point, *two* measurements are necessary (wall temperature and heat flux at two different operating points) to define a linear boundary condition in the form of Eq. (3).

In practice, especially for complex flows, the existence of this linear relationship does not hold and this is the origin of most of the discrepancies between the coupled and the uncoupled approach.

Coupled Thermal/CFD Method

Coupled methods do not assume any hypothesis in the the fluid/solid interface and therefore are well suited for solving complex flows such as turbine stator well cavities. An iterative approach is followed to satisfy temperature and heat flux continuity at fluid/solid interfaces. Giles [9] showed using 1D stability analysis for the Heat Diffusion equation that in general coupling algorithms tend to be stable imposing Dirichlet boundary conditions on the fluid domain and Neumann boundary conditions on the solid domain. That is, the temperatures obtained by the thermal code are used as boundary conditions in the CFD solver, while the heat fluxes computed with the CFD code are imposed

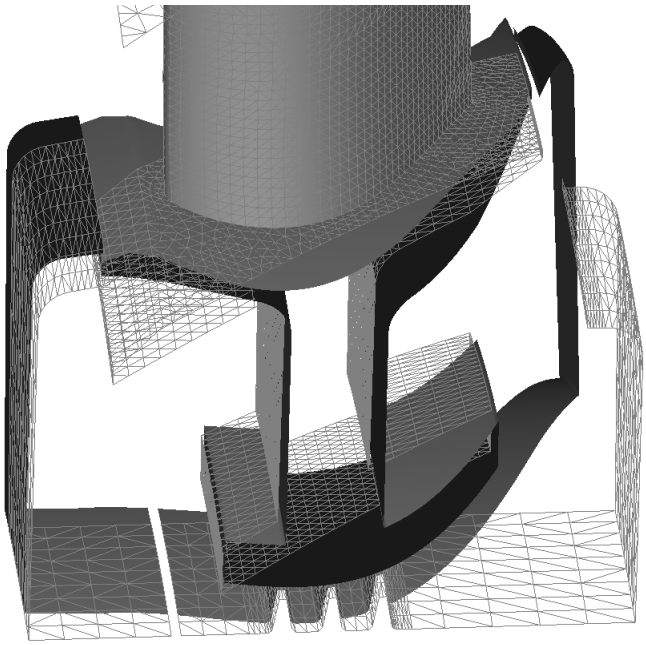

Figure 1. Data transfer between two non-conformal grids with different periodic boundaries.

to the thermal solver. We have followed this approach in this work.

This information transfer is carried in both senses at all the defined interfaces. Usually the solid and fluid surface grids are non conformal due to the disparity of the scales that need to be solved at both domains. Therefore an interpolation procedure has been developed to transfer the normal component of the heat flux and the temperature at the interface. The interpolation is not conservative in the sense that total transferred energy computed using metal and fluid wall grids could be different. In the present work the error in the worst case is lower than a 3%.

It is common that for turbomachinery 3D cases the definition of the periodic boundaries in two physically identical cases may not match because of the freedom in the definition of the periodic boundaries. This is the case when the fluid and solid grids are generated by two different systems and two different analysts (see Fig. 1). The method checks for this situation and replicates as many pitches as needed of the host surface.

The normal component of the heat flux q is obtained computing the static temperature gradient ∇T in the fluid domain

$$q = \frac{k\nabla T \cdot \mathbf{n}}{|\mathbf{n}|} \tag{4}$$

being k the fluid thermal conductivity and $\mathbf{n}$ the local normal vector to the boundary surface. The sign of $\mathbf{n}$ is not important, but the same criteria must be used in both fluid and metal domains.

Imposing directly the heat flux distribution in the thermal solver may provoke slow convergence and has a risk of stability problems in areas of high temperature gradient [17]. To address this problem, a convective boundary condition using a constant arbitrary heat transfer coefficient h is used. In this way, the boundary condition imposed in the thermal solver is

$$q_m = h\,(T_{ref} - T_m) \tag{5}$$

being q_m and T_m the local normal component of the heat flux and temperature at the metal boundary domain. T_{ref} is a local reference temperature which remain constant during each thermal solver call, but could be different for each surface node. The heat flux q_f^n computed with the fluid solver in the global iteration n is used to obtain T_{ref} :

$$T_{ref}^n = T_f^n + \frac{q_f^n}{h} \tag{6}$$

Once the thermal solver is converged, the boundary condition imposed to the CFD is directly the temperature at the walls obtained from the thermal solver solution:

$$T_f^{n+1} = T_m^n \tag{7}$$

Using Eqs. (5), (6) and (7) we obtain that

$$q_m^n - q_f^n = h\left(T_f^n - T_f^{n+1}\right) \tag{8}$$

The last expression means that if convergence is achieved ($\left|T_f^n - T_f^{n+1}\right| \to 0$), the continuity of the heat fluxes is fulfilled ($\left|q_m^n - q_f^n\right| \to 0$). Expression (7) ensures as well the continuity in the temperature field. Hence the value of h has no effect on the solution. It only affects the convergence history as we can see in equation (8). A smaller value of h results in a larger change of the wall temperature between two successive iterations. In the present work a value of 3 mW/mm^2K has been used,

Uncoupled Methodology

As it was mentioned earlier, the uncoupled approach is much faster than the coupled approach because less CFD simulations are needed to obtain a thermal solution. In this work only two CFD solutions are performed to derive the constants needed to

impose the Newton's law in the thermal solver. When running the CFD codes, constant temperatures are set on the common surfaces with the metal domains. These temperature values are a guess and could be constant in all the walls, or constant in each surface. The two CFD simulations must have different wall temperatures ($T_{w,1} \neq T_{w,2}$), typically $5K$. Once both CFD simulations are obtained, the existence of a constant heat transfer coefficient is assumed for each node at the boundaries, Eq.(3), h and T_{ref} are computed solving a linear equation system at each node. Then a distribution for the heat transfer and for the reference temperature is obtained:

$$h = \frac{dq}{dT_w} = \frac{q_1 - q_2}{T_{w,2} - T_{w,1}} \tag{9}$$

$$T_{ref} = T_{w,1} + \frac{q_1}{q_1 - q_2}\left(T_{w,2} - T_{w,1}\right) \tag{10}$$

Some numerical problems can appear if the boundary normals are undefined, typically at surface intersections, where discontinuities are likely to appear. For this reason some limiters are applied to Eqs. (9) and (10) in order to constrain the values in a valid range. In this way, no negative values are allowed for h, and if T_{ref} is out of a prescribed range, between $[173K, 3000K]$ in our case, then T_{ref} is set to $\left(T_{w,1} + T_{w,2}\right)/2$.

VALIDATION CASE DESCRIPTION

For validation purposes, experimental data taken from the Work Package 1 of the EU FP6 MAGPI project have been used. The test facility [7] consists of a two stage turbine rated a 400 kW with a generic blade geometry representative of modern gas turbines. The average stator exit Mach numbers are approximately 0.7 which gives a representative potential field at the rim seals. The two stages are approximately equally loaded and have similar geometry. The rotor stages have 78 blades and the stators 39. The design speed is 10630 rpm at a mass flow of 4.8 kg/s, inlet total pressure and total temperature are respectively 3 bar and 165 $^{\circ}C$. The rig design provides a wide range of flow features to be fitted. In this work only the so called Drive Arm geometry is used with 39 coolant delivery holes.

The 3D computational domain used for all the steady CFD simulations performed in the present work contains a single pitch of the second stator including its front and rear cavities. The disk holes has been substituted by a slot of equivalent area. Fig. 2 displays the geometry of the stator and the associated cavities. Coloured points give the instrumentation locations: yellow points indicate metal temperatures, while green points measure fluid total pressure and temperature. Measurement points are numerated to ease the discussion. As it is shown in Fig. 2, three

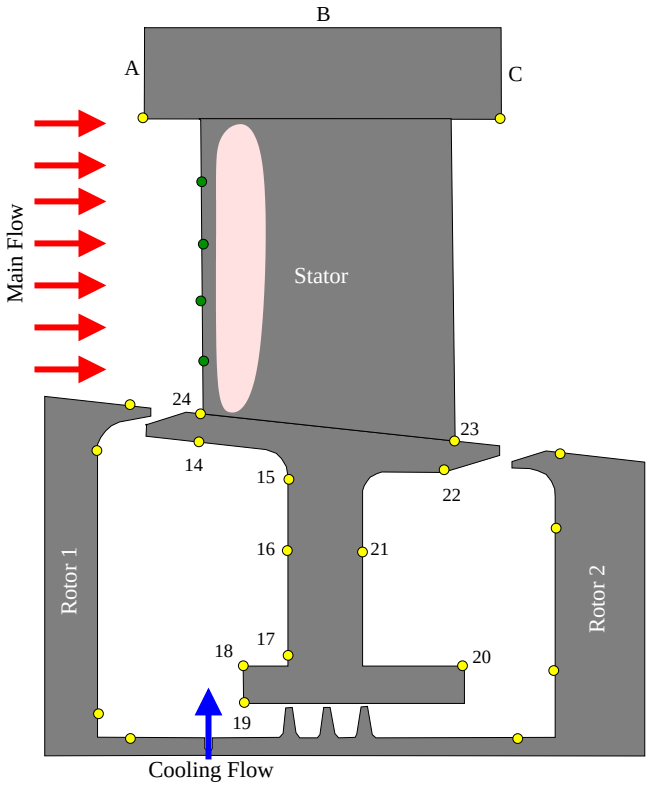

Figure 2. Schematic showing geometry and instrumentation locations

solids conform the thermal model. The two solids used to close the cavity with the neighbouring rotor blades are dummy because their temperatures are set using the experimental data. The objective of this work is to reproduce the temperatures of the static part of the cavity assuming that temperatures at the rotating walls are known. However these solids are necessary to build the CFD cavity domain. All the stator boundary conditions are computed using CFDs except for external casing surface (side B in Fig. 2), where a natural convection correlation for an horizontal cylinder taken from [5] has been used, and a constant temperature taken from the experimental data has been set at the two casing vertical surfaces (edges A and C in the Fig. 2). The grid size for the stator solid model is 13,000 nodes.

The inlet conditions for the main flow and the cooling flow are taken from the experimental data (the inlet total temperatures are about $385K$ for the main flow and $350K$ for the cooling flow). The static pressure of the outlet main flow and the total pressure of the inlet cooling flow are adjusted in order to match the measured mass flows. The $k-\omega$ turbulent model [18] has been used. The grid size of the CFD model is about 3.15 million nodes. In Fig. 3 a closeup view of the numerical model at the labyrinth seal area is shown. It may be appreciated the big difference in the grid sizes for both domains.

Following the standard approach [7], the nondimensional

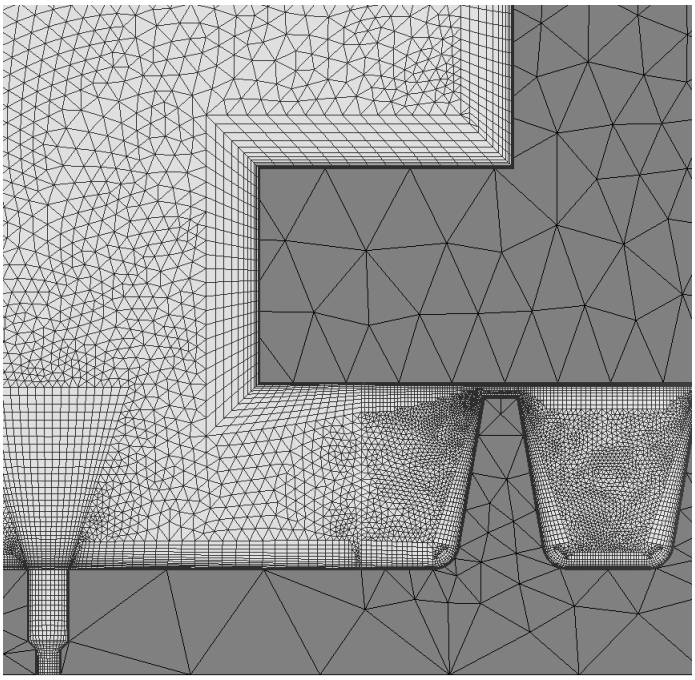

Figure 3. Grids for CFD and Metal domains at the labyrinth seal and inlet cooling flow.

mass flow rate $C_w = \dot{m}/b\mu$ within cavities are referred to the so-called disc entrainment flow $C_{w,ent}$. The viscous boundary layer of rotating disc entrains and pumps flow radially. Disc entrainment flows can be considered in relation to the flow which would be pumped by a free disc $C_{w,0}$ at the same rotational Reynolds number Re_ϕ:

$$C_{w,0} = 0.219 Re_\phi^{0.8}$$

The flow pumped by a partial disc with an inner hub was derived analytically by Chew [6], who also presented a simple fit to express the reduced flow in relation to that which would be pumped by a free disc:

$$C_{w,ent} = C_{w,0}\left[1 - \left(\frac{a}{b}\right)^5\right]$$

being a and b the disc inner and outer radius.

Experimental data in three operating conditions have been used with non-dimensionalised cooling flow rates of 0.71, 0.87 and 1.13 times the flow which would be entrained by the downstream face of Rotor 1. For the sake of clarity, these operating conditions will be referred to as the *Low*, *Mid* and *High* cases.

Case Name	T_{cold}[K]	T_{hot}[K]
Low_Hot	340.4	714.0
Low	350.4	419.2
Mid	341.2	405.5
High	327.0	403.3

Table 1. Reference temperatures.

The three cases has been run using coupled and uncoupled approaches. Because some experimental data were provided after the simulations were finished, CFD models have been run with slightly lower cooling mass flow rates than the measurements (11%, 9% and 4% respectively).

As it will be explained later, in order to assess the sensitivity to the temperature gradient between the main flow and the cooling in the mismatching between the coupled and uncoupled solutions, a fourth case call *Low-Hot* has been studied analytically since no experimental data are available. This case is similar to the *Low* case, but the inlet total temperature in the main flow has been increased by 300 *K*. The temperatures at the bottom of the cavity has been maintained and a linear variation has been applied at the rotor walls until reach the main flow-path.

RESULTS

For the four validation cases, two reference temperatures has been defined, T_{cold} and T_{hot}, being the hottest and coldest temperatures found in both domains for the coupled cases. With these values a nondimensional temperature is defined as

$$\theta = \frac{T - T_{cold}}{T_{hot} - T_{cold}} \tag{11}$$

The two reference temperatures are given for the four cases in table 1. In Fig. 4 the nondimensional temperature errors against experimental data are given for the coupled and uncoupled solutions at the location probes showed in Fig. 2. The errors are defined as

$$Error_\theta = \left|\frac{T - T_{exp}}{T_{hot} - T_{cold}}\right| = |\theta - \theta_{exp}| \tag{12}$$

It is clear that the coupled approach yields consistently a better matching with the experimental data than the uncoupled approach. The maximum errors for the coupled approach are for the *Low*, *Mid* and *High cases* 6.4%, 2.8% and 3.3% respectively. For the uncoupled solutions these errors grow up to 11.3%, 9.6% and 5.8% respectively.

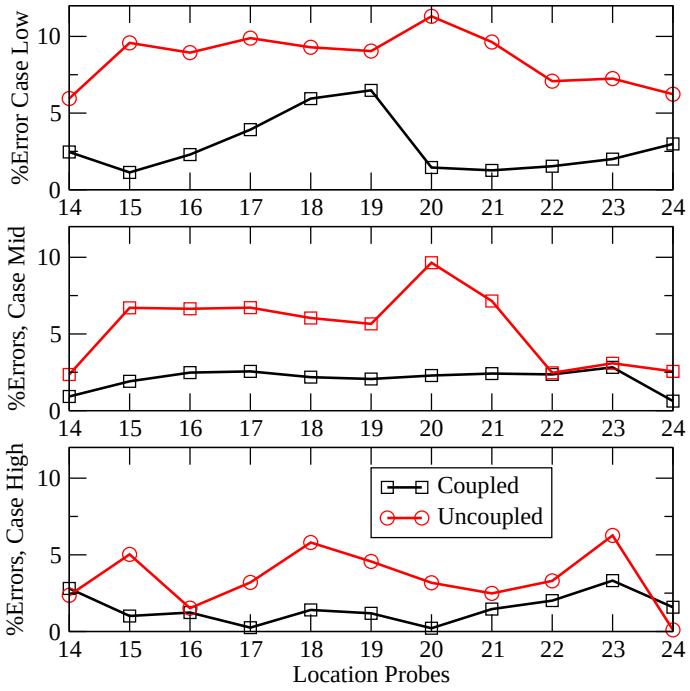

Figure 4. Comparison of the coupled (□) and uncoupled (◯) approaches against the experimental data for the *Low* (Top), *Mid* (Middle) and *High* (Bottom) cases.

Regarding the coupled solution, the worst results are obtained for the *Low* case. This can be explained because the temperature gradients in this case are higher than in the other two cases. The increment in the temperature gradient in the cavity may be explained in terms of the amount of ingested mass flow in the front cavity. The ingestion mass flow in the CFD for the *Low* case is $0.269 \cdot C_{w,ent}$, for *Mid* case is $0.06 \cdot C_{w,ent}$ and no ingestion is produced in the *High* case. The influence of the cooling mass flow in the cavity flow field can be seen in Fig. 5 where the streamlines are plotted for the three cases for the coupled solution. No big differences have been observed between these flow fields with the CFD uncoupled and uncoupled solutions. This effectively means that the flow pattern do not suffer any significant variation between both approaches. The flow structure in the front cavity is mainly formed by two counter-rotating vortices. The size of the bottom vortex increases with the cooling mass flow. For the ingestion cases, the mass flow coming from the main annulus goes towards the interstage seal zigzagging across the main two counter-rotating vortices. On the other hand, the mass flow through the interstage seal is independent of the cooling mass flow and therefore the flow structure keeps constant within the rear cavity.

Therefore it seems that when the temperature gradient increase, the accuracy of the uncoupled solutions decreases. To check the temperature gradient sensitivity, the *Low_Hot* has been

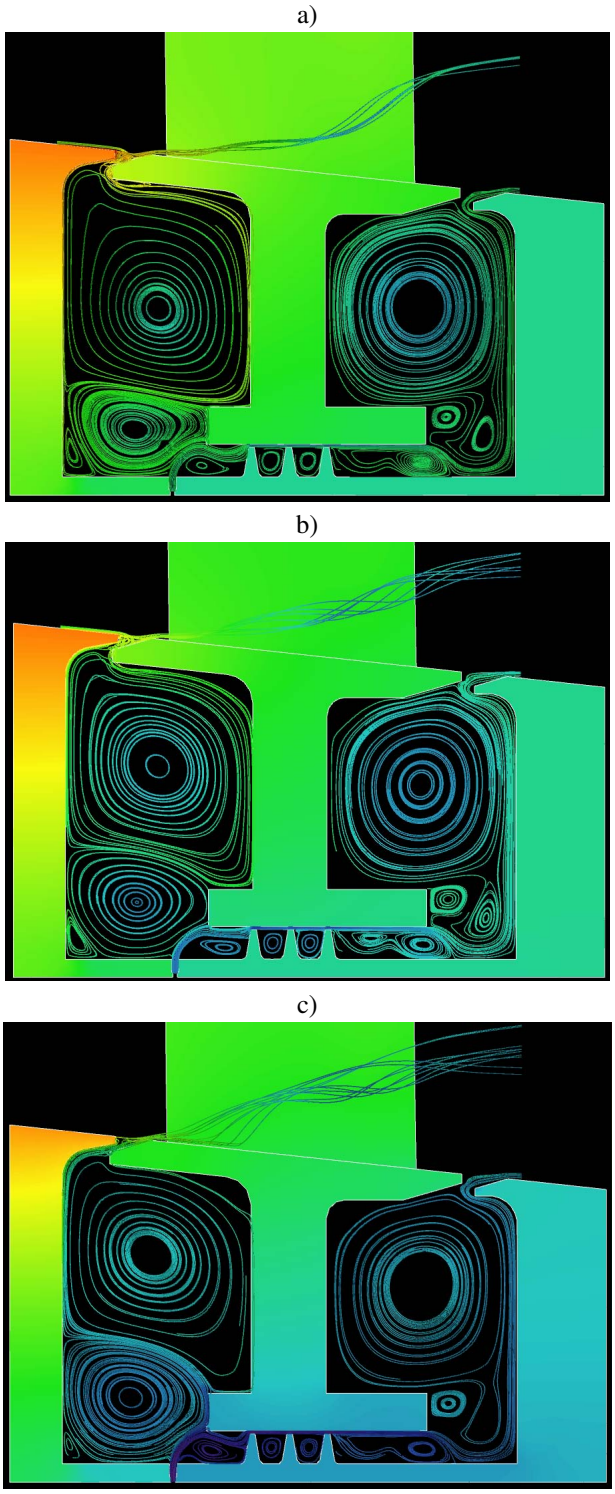

Figure 5. Streamlines for a cooling mass flow $0.71 \cdot C_{w,ent}$ (a), $0.87 \cdot C_{w,ent}$ (b) and $1.13 \cdot C_{w,ent}$ (c) of coupled cases coloured with the static temperature. The temperature range is $T \in [325K, 413K]$.

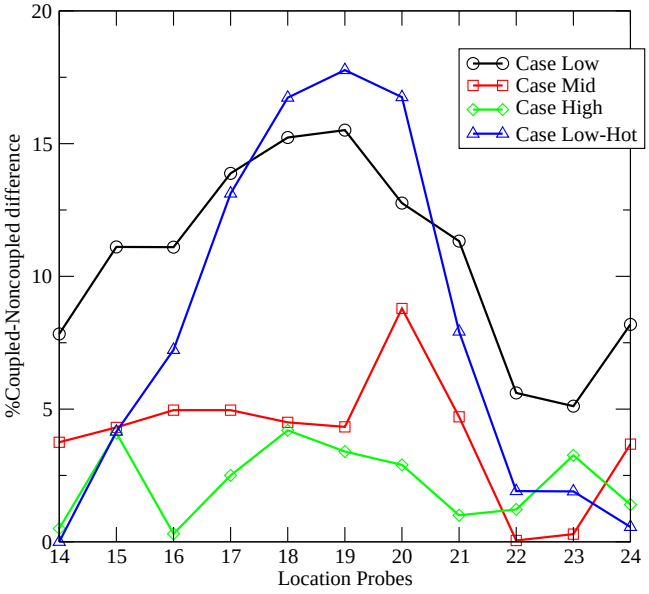

Figure 6. Percentage differences in nondimensional temperature between coupled and uncoupled solutions for *Low*, *Mid*, *High* and *Low-Hot* cases.

Case	Difference %
Low-Hot	17.8
Low	15.5
Mid	8.79
High	4.10

Table 2. Maximum differences between coupled and uncoupled solutions

used. The ingestion rate of this case is equal to the Low case, $0.269 \cdot C_{w,ent}$. Because no experimental data are available for this case Fig. 6 displays just the differences between coupled and uncoupled solutions ($100\left|\theta_{coupled} - \theta_{uncoupled}\right|$) for the four cases. In table 2 the maximum difference between the coupled and uncoupled solutions are shown. As expected, the higher difference has been obtained for the *Low-Hot* case.

Finally, for visualizing the information transferred between the two codes in the coupled approach, Figs. 7 and 8 show respectively the temperature and flux fields for the *Low* case. In the same way, in Figs. 9 and 10 the reference temperature and heat transfer coefficient for uncoupled case for the *Low* case are given. In Fig. 11 the metal nondimensional temperature difference field between coupled and uncoupled solutions for case *Low* is shown. Note that a good agreement is produced in the main flow, whereas the maximum difference (14% in nondimensionsal temperature) are seen in the front part of the stator foot.

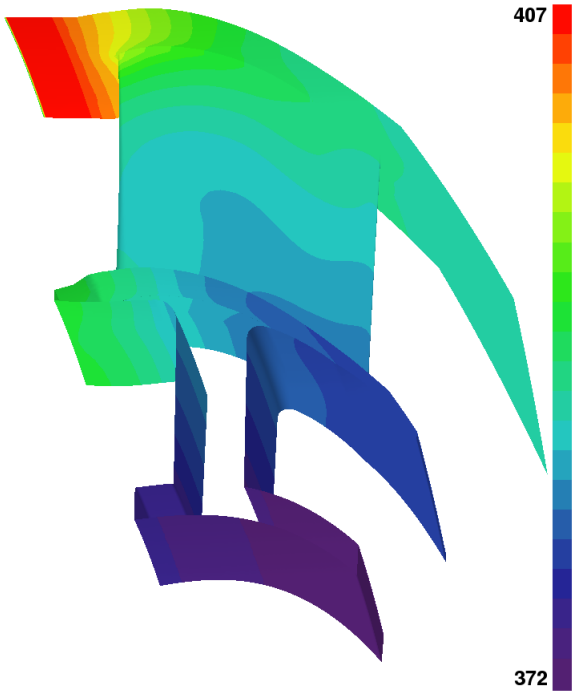

Figure 7. Temperature field (K) transferred to CFD solver for coupled case *Low* in last iteration.

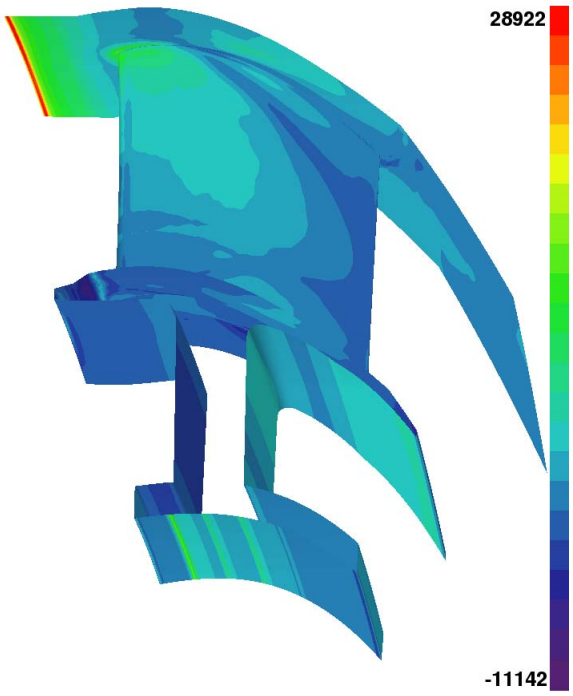

Figure 8. Heat flux field (Wm^{-2}) transferred to thermal solver for coupled case *Low* in last iteration.

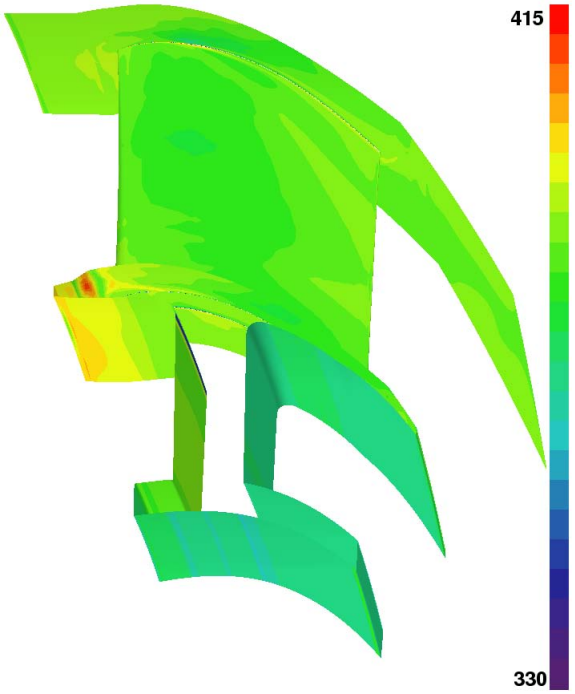

Figure 9. Reference temperature field (K) for uncoupled case Low.

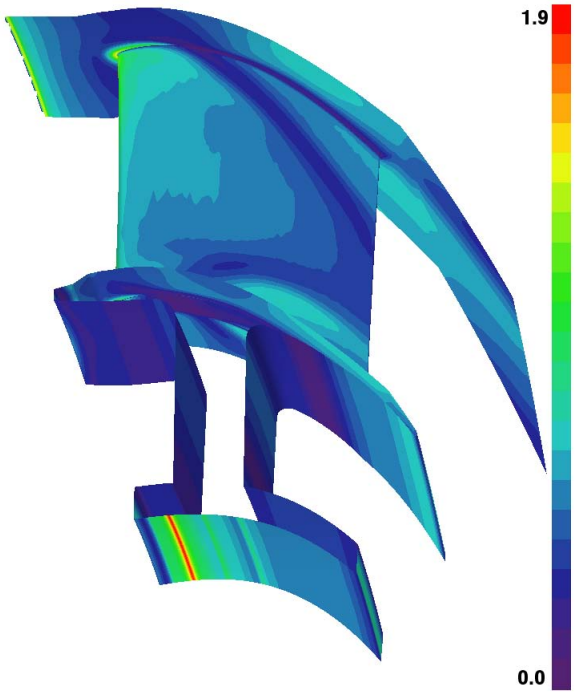

Figure 10. Heat transfer coefficient field ($mW \cdot mm^{-2}K^{-1}$) for uncoupled case Low.

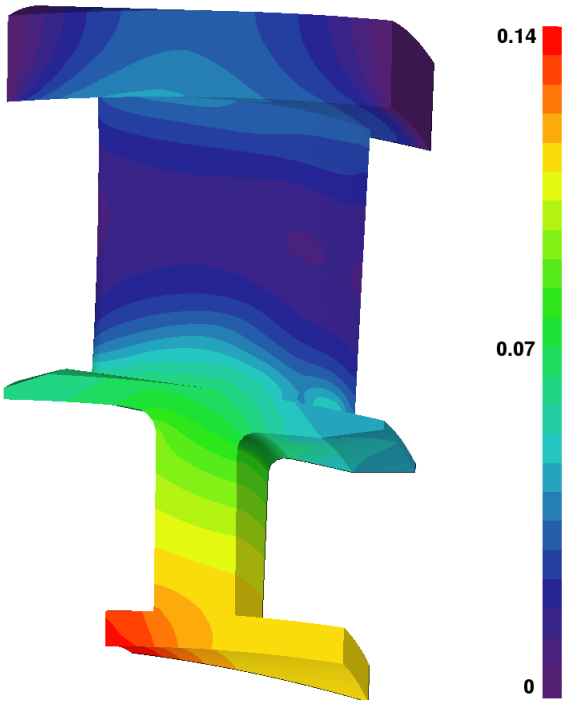

Figure 11. Metal nondimensional temperature difference field between the coupled and uncoupled approaches for case Low.

COMPUTATIONAL COST

The computational cost of coupled or uncoupled simulations are determined by the CFD runs because of the large difference in the grid size required (in this work, the mesh of the CFD model is 240 times larger than that of the thermal model). Parallel execution in a PC-cluster is required for the CFD simulations. In the coupled approach, the communication between the thermal and CFD codes is done in an automatic way. The thermal code is run in a unique cluster node, meanwhile the CFD has been run in 8 nodes.

In order to save computational cost, it is important to assign a good stop criterion for the CFD simulation defining a threshold in residual accuracy and the maximum number of iterations. In this way, when the global coupled simulation is reaching the convergence, because the CFD code is restarted form previous solution, less steps are required for achieving the CFD stop criterion. In this way, the wall-clock time needed in the first global iteration for converge the CFD solution is around 6 hours, and in the last iteration this time drops to just 5 minutes. The thermal solver needs few seconds for the convergence, and it is restarted as well from the solution of the previous global iteration.

The initial solution has been generated assuming adiabatic boundary conditions at the common walls. It would be possible to start from a better solution imposing the temperatures extracted from a lower order thermal model. For the coupled Low

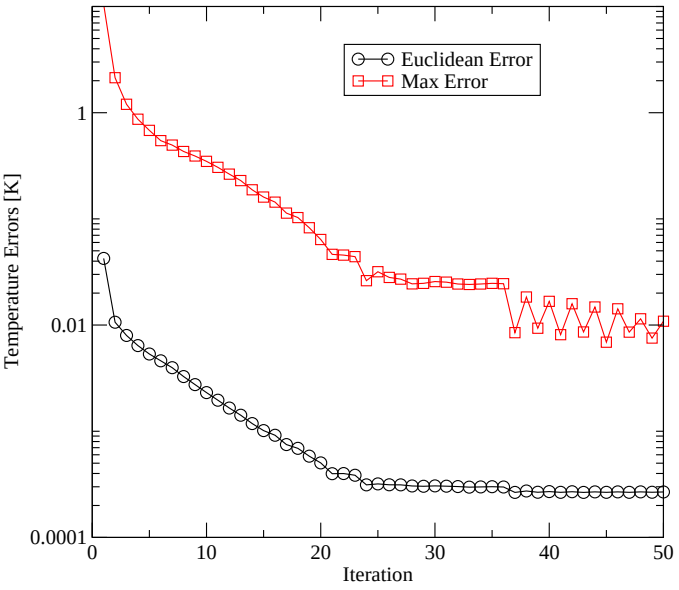

Figure 12. Coupled approach convergence history for the *Low* case.

case, the total wall-clock needed has been 30 hours to run 50 global iterations. The uncoupled case has been run in 6 hours because the two CFD models have been run in parallel.

To check the global convergence of the method several variables can be monitored. For instance, the global energy transferred at the common walls computed by the CFD domain and metals domains should be stabilized and achieved the same value at the convergence. Other possible value to check is the temperature variation between one iteration and the following. Several norms could be used, for instance the Euclidean or max norm errors:

$$T_{EucError} = \sqrt{\frac{1}{N}\sum_{i=1}^{N}\left(T_i^{n+1} - T_i^n\right)^2} \tag{13}$$

$$T_{MaxError} = \max\left(\left|T_i^{n+1} - T_i^n\right|\right) \tag{14}$$

being N the number of nodes at the common surfaces and n the global iteration. The wall temperatures T_i could be taken from the CFD or from the thermal domain because equation (7) ensures the continuity in wall temperature field. In Fig. 12 the convergence history ($T_{EucError}$ and $T_{MaxError}$) for coupled case *Low* is shown.

CONCLUSIONS

The validation of a coupled thermal/CFD method has been performed using the experimental data taken from the MAGPI project using a 3D steady stator vane with its cavities for different cooling flows. Good agreement has been obtained, with errors below the 6.5% of the nondimensional metal temperature for the worst case, which corresponds with the lower value of the cooling mass flow and the larger level of ingestion in the front cavity. If no ingestion is produced, the maximum error decreases to 3.3%.

The uncoupled approach has been assessed as well. Because it is not possible to defined a unique reference temperature inside the cavity, two CFD models are needed to define a local heat transfer coefficient and a reference temperature. The uncoupled approach is less accurate giving errors up to 11% in the nondimensional temperature. This shows that the Newton's law is not valid inside the cavity where the flow patterns are very complex. This effect is larger when high temperature gradients are generated in the cavity. To check this point, an artificial case have been run increasing the difference between hot and cold temperatures by 300K. In this case, the difference between the coupled and uncoupled runs has increased up to 18%, being 15% in the previous cases.

ACKNOWLEDGMENTS

This work was supported by the European Commission within the Framework 6 Program, Research Project Main Annulus Gas Path Interactions (MAGPI), AST5-CT-2006-030874. The authors wish to thank EU FP6 program for their support and permission to use the experimental data to validate the codes.

REFERENCES

[1] S. Alizadeh, K. Saunders, L. V. Lewis, and J. Provins. The use of cfd to generate heat transfer boundary conditions for a rotor-stator cavity in a compressor drum thermal model. In *ASME Paper No. GT2007-28333*, 2007.

[2] B. S. Baldwin and H. Lomax. Thin layer approximation and algebraic model for separated turbulent flows. In *AIAA 16th Aerospace Science Meeting*, Huntsville, Alabama, 1978.

[3] Manuel A. Burgos, Juan M. Chia, Roque Corral, and Carlos Lopez. Rapid meshing of turbomachinery rows using semi-unstructured multi-block conformal grids. *Engineering with Computers*, 26(4):351–362, 2009.

[4] Manuel A. Burgos, Jesus Contreras, and Roque Corral. Efficient edge-based rotor/stator interaction method. *AIAA Journal*, 49:19–31, 2011.

[5] A. J. Chapman. *Heat Transfer*. MacMillan, New York, third edition edition, 1974.

[6] J. W. Chew. The effect og hub radius on the flow due to a rotating disc. *Journal of Turbomachinery*, 110:417–418, 1998.

[7] D. D. Coren, N. R. Atkins, J. R. Turner, D. E. Eastwood, S. Davies, P. R. N. Childs, J. Dixon, and T. S. Scanlon. An

advanced multi-configuration stator well cooling test facility. In *ASME Paper No. GT2010-23450*, 2010.

[8] R. Corral, G. Pastor, and Jesus Contreras. Turbomachinery thermal analysis using coupled two and three dimensional models and reduced order fluid models. In *ASME Paper No. GT2011-45998*, 2011.

[9] M. B. Giles. Stability analysis of numerical interface conditions in fluid-structure thermal analysis. *International Journal of Numerical Methods in Fluids*, 24:739–757, 1997.

[10] J. B. Illingworth, N. J. Hills, and C. J. Barnes. 3d fluid-solid heat transfer coupling of an aero engine pre-swirl system. In *ASME Paper No. GT2005-68939*, 2005.

[11] K. Kusterer, D. Bohn, T. Sugimoto, and R. Tanaka. Conjugate calculations for a film-cooled blade under different operating conditions. In *ASME Paper No. GT2004-53719*, 2004.

[12] L. V. Lewis and J. I. Provins. A non-coupled cfd-fe procedure to evaluate windage and heat transfer in rotor-stator cavities. In *ASME Paper No. GT2004-53246*, 2004.

[13] A. V. Mirzamoghadam and Z. Xiao. Flow and heat transfer in an industrial rotor-stator rim sealing cavity. In *ASME J. Eng. Gas Turbines Power, 124*, pages 125–132, 2002.

[14] Y. Okita. Transient thermal and flow field in a turbine disk rotor-satator system. In *ASME Paper No. GT2006-90033*, 2006.

[15] Z. Sun, J. W. Chew, N. J. Hills, K. N. Volkov, and C. J. Barnes. Efficient finite element analysis/computational fluid dynamics thermal coupling for engineering applications. *Journal of turbomachinery*, 132, n3:031016.1–031016.9, 2010.

[16] J. A. Verdicchio, J. W. Chew, and N. J. Hills. Coupled fluid/solid heat transfer computation for turbine discs. In *ASME Paper No. 2001-GT-012*, 2001.

[17] T. Verstraete, Z. Alsalihi, and R. A. Van den Braembussche. Numerical study of the heat transfer in micro gasturbines. In *ASME Paper No. GT2006-90161*, 2006.

[18] D. C. Wilcox. *Turbulence Modeling for CFD*. DCW Industries, California, 1998.